



Alternative platinum electrocatalyst supporter with micro/nanostructured polyaniline for direct methanol fuel cell applications

Y.F. Huang, C.W. Lin*, C.S. Chang, M.J. Ho

Department of Chemical and Materials Engineering, National Yunlin University of Science and Technology, 123, Sec. 3, University Road, Douliou, Yunlin, Taiwan

ARTICLE INFO

Article history:

Received 2 October 2010
Received in revised form 6 April 2011
Accepted 7 April 2011
Available online 27 April 2011

Keywords:

Polyaniline nanofibers
Catalyst supporter
Methanol oxidation
Direct methanol fuel cells

ABSTRACT

In this study, a series of micro/nanostructured polyanilines were synthesized and their morphology-dependent electrochemical properties for acting as a catalyst supporter for direct methanol fuel cell (DMFC) applications were investigated. These micro/nanostructures include submicron spheres, hollow microspheres, nanotubes, and nanofibers. Among the four micro/nanostructures, polyaniline nanofibers (PANF) manifest their superiority in high electrochemical active surface. Accordingly, PANF is adopted as the catalyst supporter thereafter. To couple with the use of the alternative catalyst supporter, this study also investigates the effect of reductant type on morphology and electrocatalytic properties of the PANF-supported Pt particles through a chemical reduction reaction. TEM images indicate that formic acid as a reductant results in well-dispersed Pt particles on the PANF surface. On the other hand, aggregations of Pt are observable when NaBH_4 is selected as a reductant. Moreover, the methanol oxidation current density measured with the Pt/PANF electrode being prepared by using formic acid is double that by using NaBH_4 . Compared with Pt/XC-72, the Pt/PANF electrode possesses higher electrocatalytic activity and exhibits double power density. Moreover, Pt/PANF is superior to Pt/XC-72 in the aspect of operation stability based on a continuous discharge for 5 h.

© 2011 Elsevier Ltd. All rights reserved.

1. Introduction

Direct methanol fuel cells (DMFCs) are highly attractive power sources for a variety of applications, due to their high-energy efficiency, low emission, low noise, and environmentally friendly nature [1,2]. Despite these advantages, however, some problems still prevent the commercialization of DMFCs. These problems include the fuel crossover from anode to cathode, the poison of platinum catalyst, and the reliability and durability of the membrane electrode assembly (MEA). The poison of the Pt catalyst presents one of the greatest challenges for DMFCs, as it causes a significant loss in their performance [3,4]. Researchers have attempted to overcome the catalyst poison problem, including the modification of Pt with different metals and the selection of a catalyst supporter [5–9]. It has been shown that the use of polyaniline as the catalyst supporter is a simple and useful way of reducing the catalyst poison problem [10–12]. Polyaniline can form a specific interaction with Pt and helps to reduce the absorbance of CO on Pt

particles, which is a major factor leading to the poison of Pt catalyst [13].

Several recent studies reported that nanostructured polyaniline has a large accessible surface area and a low electric resistance, making it a particularly suitable catalyst supporter for promoting the catalytic ability of Pt particles. For example, Chen et al. and Guo et al. [14,15] reported that ultra-high density Pt particles can be grown on the surface of polyaniline nanofiber (PANF), and the Pt/PANF catalysts have higher methanol oxidation ability than the Pt/XC-72 carbon and the commercial E-Tek catalysts. Researchers have reported similar results using polyaniline nanotubes as supporters. For example, Rajesh et al. [16,17] reported that the Pt supported on the polyaniline nanotubes exhibited excellent catalytic activity and stability in comparison with the Pt supported on the XC-72 carbon with conventional polyaniline. Moreover, a recent study [18] reported the use of hollow polyaniline microspheres as catalyst supporters to enhance the electrocatalytic capability of the deposited metal.

Although many studies have reported the use of PANI as catalyst supporters, their shape-dependent electrochemical properties have not been systematically studied. The morphology of micro/nanostructures plays an important role in their electrochemical properties, such as electronic conductivity, effective surface area, and interfacial charge transfer resistance [19]. Requirements for a suitable catalyst supporting material include good electric

* Corresponding author at: Department of Chemical and Materials Engineering, National Yunlin University of Science and Technology, 123 Section 3, University Road, Douliou, Yunlin 640, Taiwan. Tel.: +886 5 534 2601x4613; fax: +886 5 531 2071.

E-mail address: lincw@yuntech.edu.tw (C.W. Lin).

conductivity, high specific surface area, and high stability in acid media. On the other hand, although the previous studies reported that using polyaniline nanostructures as supporters can significantly enhance Pt catalytic properties [14–17,20,21], it is worth noting that none of them investigated the single cell performance of these Pt/PANI nanocatalysts. To our best knowledge, only one study reports the test results of DMFC performance with PtRu/PANI and PtRu/C catalysts [22,23]. However, that study draws an inconsistent conclusion that a lower performance of PtRu/PANI is obtained when compared with PtRu/C [23].

To clarify the advantage of using adequate nanostructured polyaniline as catalyst supporter for DMFC applications, this study aims to investigate the electrochemical properties of polyaniline with different micro-/nano-structures (i.e. submicron spheres, hollow microspheres, nanofibers, and nanotubes) to determine a most suitable shape of Pt supporter. Morphology and catalytic ability of Pt particles deposited on the synthesized PANI supporter through different reduction agents are also investigated. To demonstrate the benefit of using a PANI nanostructure as a Pt supporter, we make a series of comparative study on the single cell tests of DMFC in terms of polarization curve and operation stability under the use of identical Pt catalyst supported on the PANI nanostructure and the carbon black XC-72, respectively. It is worthy to remind that the reason why we deposit Pt rather than Pt–Ru on PANI as the electrocatalyst for DMFC in the current study is to avoid complicating the benefit of diminishing the Pt poison with PANI. After all, the use of Pt–Ru as catalyst has manifested an effect upon lowering the Pt poison for DMFC operations [5,6].

2. Experimental

2.1. Materials

Aniline monomers ($\geq 99.5\%$, Fluka) and ammonium persulfate (APS, Riedel-de Haën) were used to synthesize polyaniline nanofibers, nanotubes, submicron spheres, and hollow microspheres with the introduction of hydrochloric acid (37%, MERCK-GR), Methanol (99.8%, Riedel-de Haën), 1,6-hexandiol (99%, Aldrich), or 1-propanol (98%, J.T. Baker) in the reaction solutions. Potassium tetrachloroplatinate (II) (K_2PtCl_4 , 99.9%), the precursor of platinum, was purchased from Acros Organics. The reduction agents – formic acid (98%) and sodium borohydride ($NaBH_4$, 98%) – were purchased from Acros Organics. Vulcan XC-72 carbon black was obtained from Cabot Company. Pt/C (50% Pt on carbon black—Alfa Aesar, USA) was used as a cathode electrocatalyst. All chemicals were used as received without further purification.

2.2. Synthesis of polyaniline micro/nanostructures

The reactions were implemented in a 20-mL vial. The preparation of nanofibers typically involved mixing an aqueous solution of aniline in 1 M HCl acid (5 mL) and another oxidant (ammonium peroxydisulfate) solution in the same doping acid (5 mL). The solutions were then poured rapidly into a glass vial and shaken vigorously for 30 s, and then put in an ultrasonic water bath (5210, Branson, USA) at 60 °C. The reaction was executed at a molar ratio of [ANI]/[APS] equal to 0.8:1 and the concentration of aniline was 0.2 mol L^{-1} . The nanotubes, hollow microspheres, and submicron spheres were synthesized with the same procedure, using the acid-free 1 M methanol, 1 M 1-propanol, and 2 M 1,6-hexandiol acid-free solutions, respectively. The reaction temperature for nanotubes, submicron spheres, and hollow microspheres remained at 0 °C. The resulting PANI samples were isolated by gravity filtration and washed in de-ionized water. Finally, the products were

dried in an oven at 50 °C for 1 day. The morphologies of these micro/nanostructures were executed with a field emission scanning electron microscope (FE-SEM; JSM-7401F, JEOL, Japan) and a transmission electron microscopy (TEM; JEM-1400, JEOL, Japan) operating at 120 kV.

2.3. Deposition of Pt particles on the PANI and XC-72 carbon black supporters

The catalyst supporters (PANI or XC-72 carbon black) were firstly dispersed in 10.3 mL of a K_2PtCl_4 aqueous solution (4.6 mM) in a 20 mL vial, followed by the addition of 2.5 mL formic acid (99%) in the solution to prepare the PANI- or XC-72-supported Pt catalysts. These mixtures were stirred at room temperature for 16 h to reduce the Pt precursors completely. Then, the solution was isolated using gravity filtration and washed several times with deionized water. For comparison, a similar reaction was performed by using the K_2PtCl_4 solution and 2.8 mL of 0.05 M $NaBH_4$ as reduction agent. UV–vis spectrophotometer (Lambda 850, Perkin Elmer, USA) was used to identify the completion of reaction of K_2PtCl_4 during the reduction process.

2.4. Electrochemical characterization of PANI, Pt/PANI, and Pt/XC-72

The cyclic voltammetry curve of the resulting polyaniline micro/nanostructures and the Pt catalysts supported on PANI and XC-72 carbon black were conducted with a three-electrode setup. The working electrode with a circular area of 1 cm^2 was prepared as follows. The PANI micro/nanostructures, Pt/PANI or Pt/XC-72 were, respectively, mixed ultrasonically with isopropanol in a glass vial with a weight ratio of 1:30. Then, a suitable amount of Nafion[®] solution was added to the dispersion and mixed until a uniform paste was obtained. The weight ratio of Pt plus catalyst supporter (i.e. PANI micro/nanostructures, Pt/PANI or Pt/XC-72) to Nafion is 1:1.34. This ink was then spread on the surface of the gas diffusion media (15% wet proof, HEPHAS energy, Taiwan) and dried in an oven at 60 °C. Besides, the weights of electrode before and after the coating of slurries were measured carefully to determine the exact quantity of polyaniline or Pt/polyaniline in the electrode and the measured weight was also used to normalize the CV curves. Ag/AgCl and platinum wire were used as the reference and counter electrode, respectively. The cyclic voltammetry curves were obtained in a 1 M methanol and 0.5 M H_2SO_4 solution. The scan range was from -0.2 to 1.0 V versus Ag/AgCl, and the scan rate was 50 mV s^{-1} .

2.5. Preparation and evaluation of direct methanol fuel cells

The anode was fabricated using gas diffusion media as a supporter with a given metal loading of 3 mg cm^{-2} . The Pt particles were deposited on the PANI nanostructures and XC-72 carbon black to be anode catalyst, respectively. The cathode was prepared by using a carbon-supported Pt catalyst (50% Pt on carbon black—Alfa Aesar, USA) with a metal loading of 3 mg cm^{-2} . The added Nafion[®] as binder in both anode and cathode is 10 wt%. 2 M methanol solutions were fed at a fixed rate of 3 mL min^{-1} and the oxygen flow rate was fixed at 100 SCCM. The pressure at the cathode side is one atmosphere. The fabrication procedures and conditions of the MEA were set according to the previous literature, using the Nafion[®] 115 as the proton conducting membrane [24]. The DMFC performance with an active area of 6.25 cm^2 was evaluated utilizing a fuel cell test station (Model 2200, MACCOR, Inc., USA).

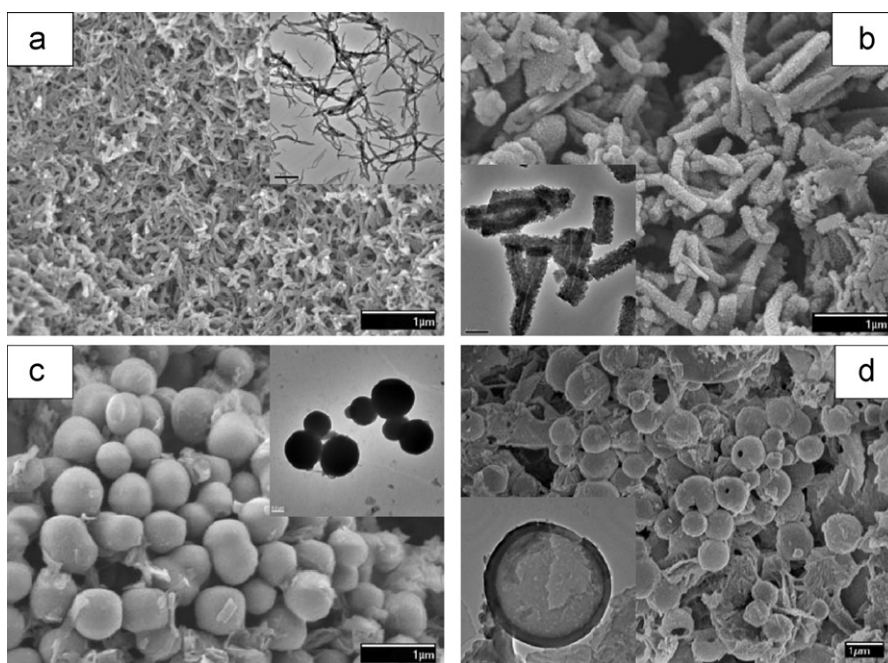


Fig. 1. SEM and TEM (corner) images of polyaniline micro/nanostructures: (a) nanofiber, (b) nanotubes, (c) submicron spheres, and (d) hollow microspheres. The reaction time for nanofibers and nanotubes is 90 min; the reaction time for submicron spheres and hollow microspheres is 45 min. The scale bar of the TEM image is 500 nm for nanofibers and 200 nm for the others, respectively.

3. Results and discussion

3.1. Synthesis and characterization of polyaniline micro/nanostructures

Fig. 1(a) and (b) shows the SEM images coupled with TEM images (placed at corner) of the PANI micro/nanostructures synthesized in different polymerization conditions. As Fig. 1(a) shows, the polymerization of aniline monomers in 1 M HCl solution at 60 °C can produce polyaniline nanofibers with a diameter of 60–80 nm. However, Fig. 1(b) shows that the polymerization of aniline in 1 M methanol acid-free solutions at 0 °C led to the formation of nanotubes with an outer diameter of 200 nm and an inner diameter of 0–50 nm. Fig. 1(c) and (d) shows that PANI submicron spheres with an outer diameter of ~400 nm and hollow microspheres with an outer diameter of ~1 μm and a thickness of 50 nm can be obtained from 1,6-hexandiol and 1-propanol acid-free solutions, respectively. These results agree well with our previous findings regarding the different growth routes of aniline monomers in different polymerization environments and conditions [25–28]. The different growth routes can therefore produce different morphologies of the polyaniline micro/nanostructures. However, the details of state-of-the-art of morphology control of polyaniline nanostructures are beyond the scope of the current study and can be referred to our previous publications [25–28].

Fig. 2 presents the CV curves of different PANI micro/nanostructures in a 1 M methanol and 0.5 M H₂SO₄ aqueous solution. All PANI samples exhibit the electrochemical activities that resulted from a typical redox response. Redox peaks at around 0.25 V and 0.7 V serve for the conversion of leucoemeraldine to emeraldine, and emeraldine to pernigraniline, respectively. The peak at 0.65 V corresponds to the redox reaction of degradation products (hydroquinone to quinone) [29,30]. As can be observed in Fig. 2, the PANI nanofibers are superior to nanotubes, submicron spheres, and microspheres in the aspect of current density. This higher current density stands for the higher effective surface area that is accessible to electrolytes [31]. Specifically, previous studies

have reported that the fibrous polyaniline may have a higher molecular weight than that of nanotubes and spheres [32–34]. Regarding this, we consider here that the difference in current density of the polyaniline species may be due to their different morphologies and/or molecular weights, which results in different electrochemical surface area. Besides, as there is a charge transfer energy barrier between the PANI micro/nanostructured supporter and the electrode substrate (i.e. carbon cloth in this case), this higher current density of nanofibers may be attributed to a close surface contact between the nanofibers and the electrode substrate as well as higher surface area [19]. These characteristics are favorable for a catalyst supporter to fabricate highly efficient electronic devices. Accordingly, this study selected the PANF as the catalyst supporter for DMFC applications hereafter. In order to pursue an optimum electrode capability, this study investigated the effects of the reduction agent type and the PANF amount on the electrocatalytic properties of the Pt/PANF catalysts.

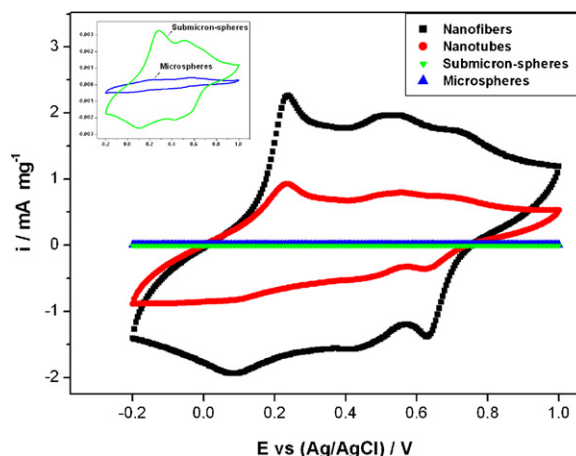


Fig. 2. Cyclic voltammogram curves of polyaniline micro/nanostructures in 1 M CH₃OH and 0.5 M H₂SO₄ solutions.

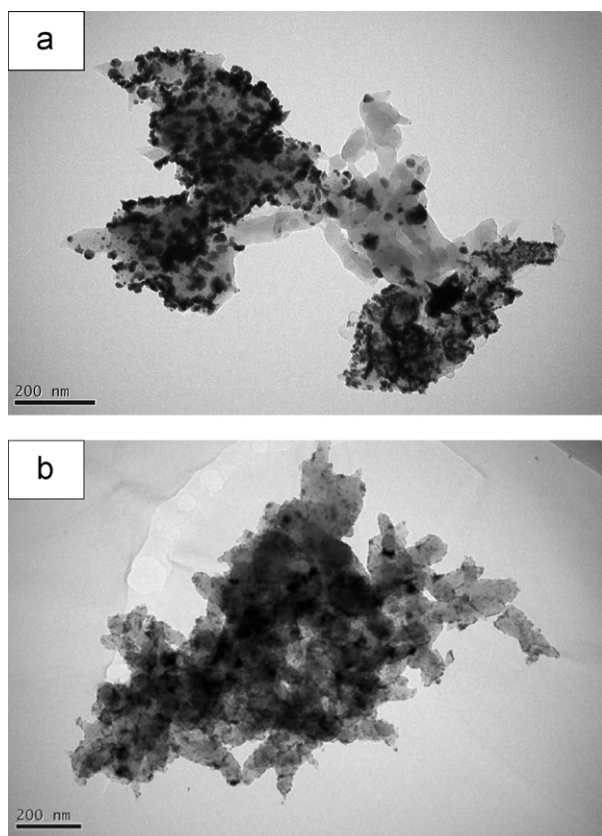


Fig. 3. TEM images of PANF (5 mg) supported Pt catalysts fabricated with different reduction agents.

3.2. Effects of reductant type on the morphology and oxidation ability of the resulting Pt/PANF catalysts

Fig. 3 shows TEM images of the PANF-supported Pt catalysts using different reduction agents. Fig. 3(a) shows aggregated Pt particles on the PANF obtained from using NaBH_4 as the reduction agent. On the other hand, using formic acid as the reduction agent can yield well-dispersed Pt particles on the PANF, as shown in Fig. 3(b). Fig. 4 shows UV–vis spectra of the reaction solutions obtained before and after the reduction process (the PANF

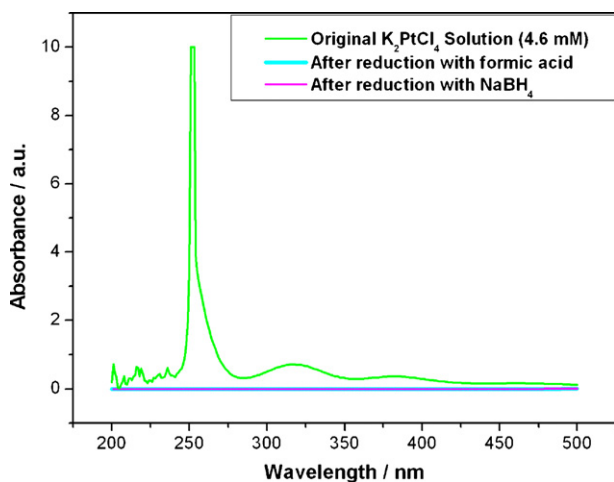


Fig. 4. UV–vis spectra of the reaction solutions obtained before and after the reduction process with addition of 5 mg PANF.

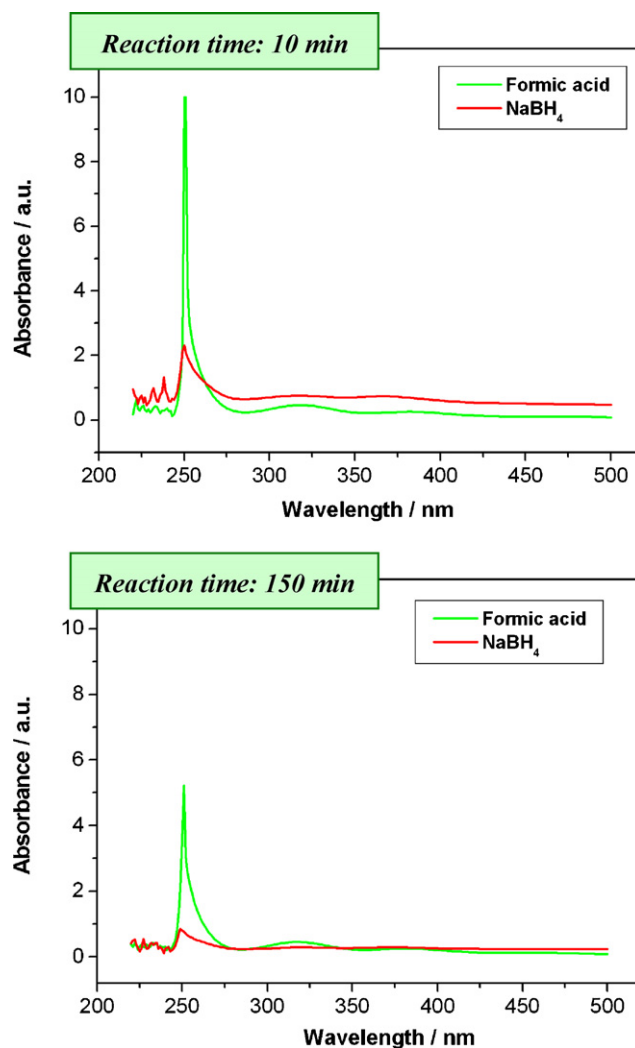


Fig. 5. UV–vis spectra of the reaction solutions obtained at different reaction stages with the using of different reduction agents.

in the solutions were filtered out). A sharp peak at 253 nm was observed from the pre-reaction solution and which can be related to the absorbance of PtCl_4^{2-} ions [35]. However, after the reduction of PtCl_4^{2-} by using formic acid or NaBH_4 as reduction agent, the peak at 253 nm disappeared. These results indicate that both formic acid and NaBH_4 can completely reduce the Pt^{2+} ions into Pt atom during the reaction process. Thus, the Pt weight ratio of the obtained Pt/PANF in the solutions with an adding PANF amount of 5 mg was calculated to be about 66.5% [15]. To further identify the composition of these Pt/polyaniline materials, this study used EDX technique to analyze the content of Pt in the Pt/PANI composite [36–38]. As Table 1 shows, the Pt weight percentages in both the Pt/PANI composites using the different reductants are quite similar and satisfactorily closed to the theoretical value (i.e. 66.5%) which is calculated based on the Pt precursors being reduced completely and the entire reduced Pt particles are incorporated into the Pt/PANI composite. Accordingly, it can be inferred that both different reduction agents can reduce the same amount of Pt on the PANF supporters, even the resulting morphologies of the PANF-supported Pt particles are significantly different. The different morphology may be attributed to the different reduction rate of the Pt precursor with the use of different reductants. As Fig. 5 shows, NaBH_4 leads to a higher reduction rate than formic acid. The absorbance of the peak at ~ 250 nm with the NaBH_4 is only one-fifth

Table 1
The EDX analysis results of the Pt/PANF compositions using different reductants.

Type of reductant	Weight ratio (%)					Atomic ratio (%)				
	C	N	Cl	Pt	Total	C	N	Cl	Pt	Total
Formic acid	27.98	4.23	0.52	67.27	100.0	77.88	10.11	0.49	11.53	100.0
NaBH ₄	30.73	3.60	1.08	64.59	100.0	80.53	8.09	0.96	10.42	100.0

to that with the formic acid at the reaction time of 10 min. The higher reduction rate from NaBH₄ may lead to a higher concentration of Pt nucleate formed at the initial reaction stage and thus leads to the aggregation of Pt particles during the reaction process [39]. In contrast, the lower reduction rate from formic acid may allow the as-synthesized Pt particles to be deposited on the polyaniline surface and thus prevent the aggregation of metal particles during the reaction process [40,41]. We therefore infer that the relatively homogenous morphology of the Pt particles with the use of formic acid can be ascribed to the lower reducing rate.

On the other hand, it is worth noting that these different morphologies of Pt particles can lead to different methanol oxidation abilities of the Pt/PANF catalysts. Fig. 6 shows the CV curves of Pt/PANF catalysts obtained from the use of different reduction agents. As can be seen, formic acid resulted in Pt/PANF catalyst with a significantly higher current peak corresponding to the oxidation of methanol (0.7 V), which is about two times higher than that of the Pt/PANF catalyst obtained by using NaBH₄. The higher electrocatalytic surface (owing to the well-dispersed and smaller Pt particles on the PANF surface) is responsible for the higher methanol oxidation current peak, as it provides a higher accessible surface to the electrolyte for the Pt particles [14]. In short, the above results indicate that the use of formic acid as a reduction agent helps the formation of uniformly distributed Pt particles on the PANF surface, and it is the well dispersed morphology of Pt promoting the methanol oxidation ability of Pt/PANF catalysts.

3.3. Effects of PANF amount on the catalytic ability of Pt/PANF

In examination of the advantages of using PANF as a Pt supporter, this study investigated the catalytic properties of Pt/PANF fabricated with the addition of different PANF amounts in the reaction solutions. Fig. 7 shows the CV curves of the Pt/PANF catalysts fabricated with the addition of different PANF amounts in the K₂PtCl₄ solutions, ranging from 2.5 to 10 mg, at the same Pt loading amount in the electrodes. As can be observed, regardless of the

amounts of PANF, all Pt/PANF catalysts show a similar methanol oxidation current peak at 0.7 V in the forward scan. However, a smallest current peak at 0.47 V during the reverse scan can be obtained with the addition of 10 mg PANF in the reaction solution. This peak corresponds to the removal of the incompletely oxidized carbonaceous species formed in the forward scan. Moreover, after oxidizing in the backward scan, these carbonaceous species generally take the form of linearly bonded Pt=C=O, which is the primary factor leading the poison of the Pt catalyst [42,43]. These results indicate that the increase of PANF amount in the reaction solutions helps to prevent the formation of linearly bonded Pt=C=O on the Pt particles and consequently enhances the CO tolerance of Pt catalyst.

These different CO tolerance-related behaviors may be due to the different Pt loading densities on the PANF surfaces. Fig. 8 shows the TEM image of the Pt/PANF catalysts prepared with adding different amounts of PANF to the reaction solutions. Fig. 8(a) shows a homogeneous Pt particle deposited on the PANF with the adding of 10 mg PANF to the reaction solution. However, Fig. 8(b) shows that decreasing the PANF amount to 2.5 mg leads to an ultra high density of Pt particles with the formation of a thicker Pt particle layer on the PANF surface. It is worth noting that this thicker Pt layer on the PANF surface may block the interaction between the outside Pt particles and the PANF supporters. The specific interaction formed between Pt and PANI helps prevent the adsorption of CO on the Pt particle [44,45]. Accordingly, it is reasonable to suggest that a suitable amount of Pt with a homogeneous distribution on the PANF surface enhances the catalyst poisoning tolerance of the Pt/PANF catalyst, and can be achieved simply by adjusting the PANF loading amount in the reaction solution.

Along with the successful improvement of the catalytic ability and poisoning tolerance of the PANF-supported Pt catalysts, this study compares the associated catalytic properties of the PANF-supported Pt with commercial XC-72 carbon black-supported Pt to demonstrate the advantage of using PANF as Pt supporters for DMFC applications.

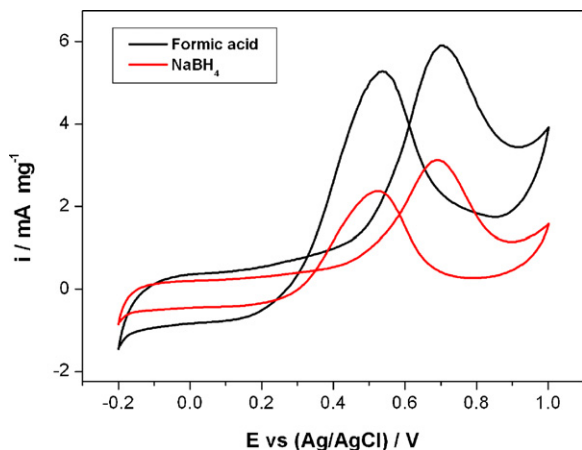


Fig. 6. Cyclic voltammograms of PANF supported Pt catalysts fabricated with different reduction agents in 1 M CH₃OH and 0.5 M H₂SO₄ solutions with addition of 5 mg PANF.

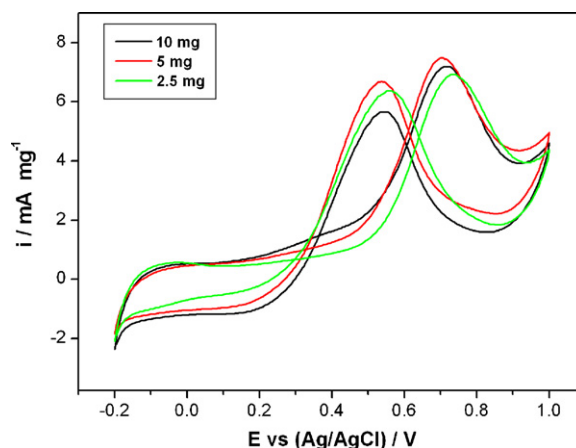


Fig. 7. Cyclic voltammograms of PANF supported Pt catalysts fabricated with the addition of different PANF amounts in 1 M CH₃OH and 0.5 M H₂SO₄ solutions.

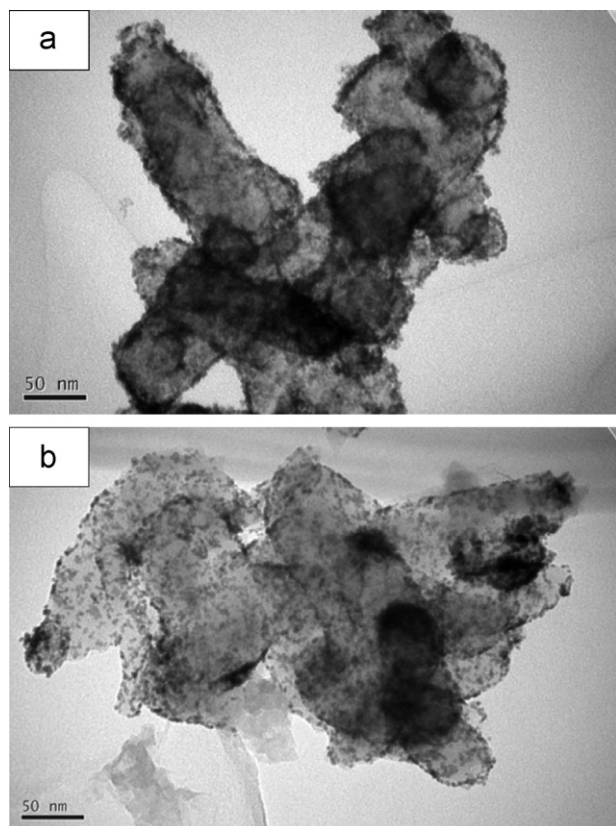


Fig. 8. TEM images of (a) 10 mg and (b) 2.5 mg PANF supported Pt catalysts.

3.4. Comparison of electrochemical properties of Pt/PANF and Pt/XC-72

Fig. 9 shows the CV curves of the commercial XC-72 carbon and PANF-supported Pt catalysts in 1 M methanol and 0.5 M H_2SO_4 solutions. The PANF-supported Pt catalysts show a slightly higher oxidation current (0.7 V) than that of the XC-72-supported Pt catalysts in the forward scan, indicating that the PANF-supported Pt catalysts have better methanol oxidation ability. However, in the reverse scan, the PANF-supported Pt catalyst exhibits a significantly lower current peak (0.47 V). Consequently, the Pt/PANF shows a significantly higher I_f/I_b ratio than that of Pt/XC-72. The I_f/I_b ratios for the Pt/PANF and Pt/XC-72 catalysts are 1.45 and 0.87, respectively.

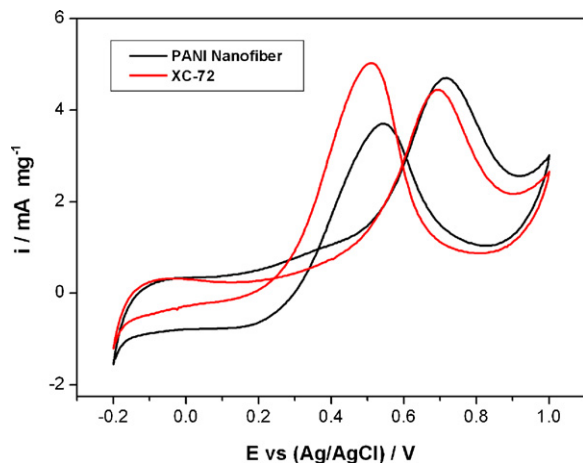


Fig. 9. Cyclic voltammograms of PANF and XC-72 supported Pt catalysts in 1 M methanol and 0.5 M H_2SO_4 solutions. The added amount of PANF and XC-72 is 10 mg.

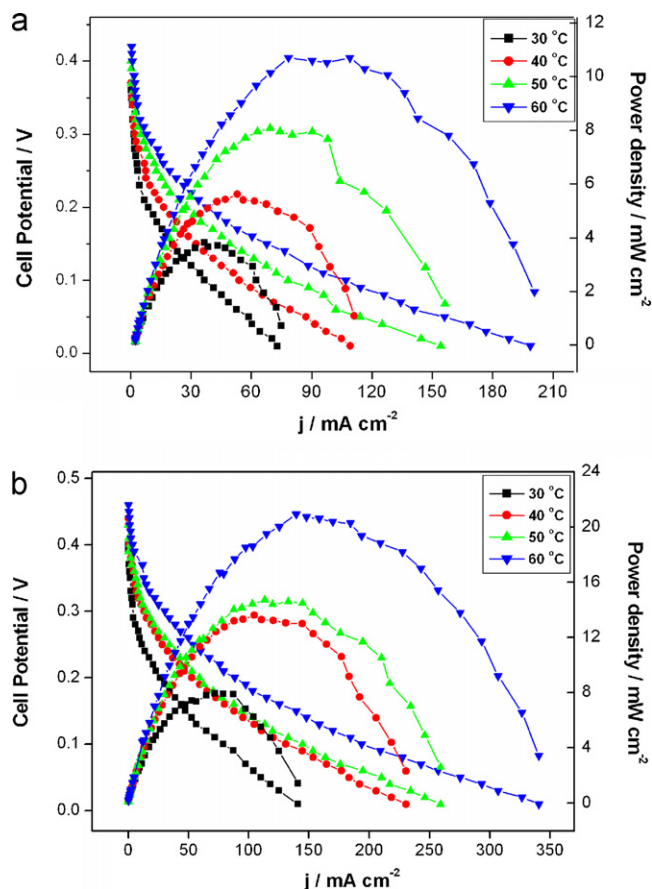


Fig. 10. Polarization curves of the DMFC using (a) XC-72 and (b) PANF supported Pt catalysts as anode. These catalysts were produced with the addition of 10 mg PANF or XC-72 in the reaction solution.

The higher I_f/I_b ratio indicates that the Pt/PANF catalyst has a better ability to oxidize methanol to carbon dioxide [42,43]. Accordingly, it is reasonable to infer that the use of PANF as a catalyst supporter can enhance the Pt catalyst to possess better methanol oxidation ability and higher poisoning tolerance than XC-72, and these are significant characteristics related to the performance and operation stability of DMFC.

Fig. 10 shows the polarization curves of the PANF- and XC-72-supported Pt catalysts as anode in DMFC with the feeding of 2 M methanol and oxygen at different temperatures. With the increase of cell temperature from 30 to 60 °C, the Pt/XC-72 catalyst demonstrates a consistent improvement in DMFC performance from 4 to 11 mW cm^{-2} , as can be seen in Fig. 10(a). However, when using Pt/PANF as the anode catalyst, polarization curves in Fig. 10(b) indicate that an increase of cell temperature from 30 to 60 °C results in an increase of power density from 8 to 22 mW cm^{-2} . It should be noted that the apparently low current densities measured for both Pt/PANF and Pt/XC-72 are due to the use of Pt instead of Pt/Ru alloy as catalyst in this preliminary study of DMFC tests. A comparison between Fig. 10(a) and (b) indicates that the power densities obtained from the Pt/PANF catalyst are all twice as high as that of the Pt/XC-72 at each corresponding temperature. These results manifest that the use of PANF as a catalyst supporter can efficiently enhance the performance of DMFC.

On the other hand, note that the DMFCs may yield a significant difference in performance stability if different anode catalysts are used. Fig. 11 presents the DMFC performances of the Pt/XC-72 and Pt/PANF catalysts obtained before and after the discharge at 0.3 V and 50 °C for 5 h. As can be seen in Fig. 11(a), the cell with Pt/XC-72 catalyst experiences a serious irreversible decline of power density

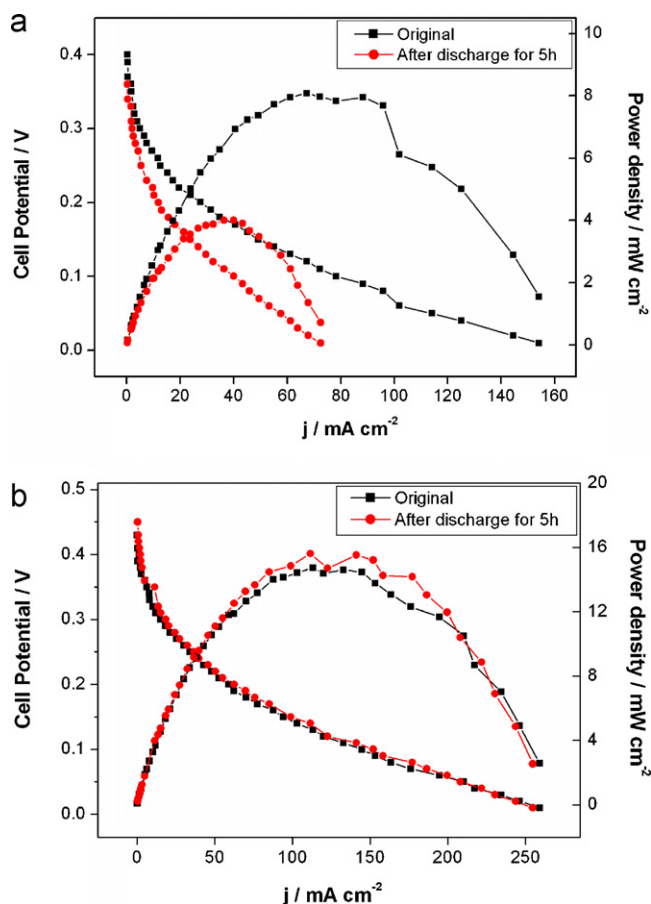


Fig. 11. Polarization curves of the DMFC using (a) XC-72 and (b) PANF supported Pt catalysts as anode after a continuous discharge at 0.3 V and 50 °C for 5 h. These catalysts were produced by adding 10 mg of PANF or XC-72 in the reaction solution.

from 8 to 4 mW cm⁻². On the contrary, a stable performance at ~15 mA cm⁻² is observable in Fig. 11(b) when Pt/PANF is used as the anode catalyst. It implies that the cell performance with Pt/PANF can be as high as about four times that with Pt/XC-72 after the continuous operation process of 5 h. These results are well correlated to the higher catalyst poisoning tolerance of the PANF-supported Pt catalysts (Fig. 9) and demonstrate that using Pt/PANF as an anode catalyst can efficiently improve the operation stability of DMFC.

4. Conclusions

This study investigates the morphology-dependent electrochemical properties of polyaniline micro/nanostructures as catalyst supporters in DMFC applications. Polyaniline nanofibers with higher electrochemical surface area and lower resistance of charge transfer to electrode manifest themselves to be highly suitable candidate. Well dispersed Pt particles on the PANF surface can be achieved by using formic acid as a reduction agent and can therefore enhance the catalytic ability of Pt. The I_f/I_b ratio from the CV curve for the Pt/PANF and Pt/XC-72 catalysts is 1.45 and 0.87, respectively, indicating the use of PANF as a catalyst supporter renders the Pt catalyst better methanol oxidation ability and higher poi-

soning tolerance. Measurements of DMFC test show that the use of PANF as Pt supporter in anode can yield twofold higher power density and better operation stability as compared to the use of XC-72. This study demonstrates an alternative and efficient way to enhance both methanol oxidation ability and CO poisoning tolerance of Pt through adopting PANF as a catalyst supporter coupled with formic acid as a reduction agent.

Acknowledgement

The authors are grateful to the National Science Council of Taiwan (ROC) for the financial support of this work under Grant no. 99-2221-E-224-069-MY2.

References

- [1] B.D. McNicol, D.A.J. Rand, K.R. Williams, *J. Power Sources* 83 (1999) 15.
- [2] X. Ren, P. Zelenay, S. Thomas, J. Davey, S. Gottesfeld, *J. Power Sources* 86 (2000) 111.
- [3] B. Beden, F. Hahn, S. Juanto, C. Lamy, J.M. Leger, *J. Electroanal. Chem.* 225 (1987) 215.
- [4] L. Niu, Q.H. Li, F.H. Wei, X. Chen, H. Wang, *Synth. Met.* 139 (2003) 271.
- [5] R. Venkataraman, H.R. Kunz, J.M. Fenton, *J. Electrochem. Soc.* 150 (2003) A278.
- [6] C. He, H.R. Kunz, J.M. Fenton, *J. Electrochem. Soc.* 150 (2003) A1017.
- [7] X. Zhang, F. Zhang, K. Chang, *J. Mater. Sci.* 39 (2004) 5845.
- [8] Y.M. Wu, W.S. Li, J. Lu, J.H. Du, D.S. Lu, J.M. Fu, *J. Power Sources* 145 (2005) 286.
- [9] L. Huang, W. Tang, T. Wen, *J. Power Sources* 164 (2007) 519.
- [10] M. Gholamian, J. Sundaram, A.Q. Contractor, *Langmuir* 3 (1987) 741.
- [11] M. Gholamian, A.Q. Contractor, *J. Electroanal. Chem.* 289 (1990) 69.
- [12] K.M. Kost, D.E. Bartak, B. Kazee, T. Kuwana, *Anal. Chem.* 60 (1988) 2379.
- [13] C. Lamy, A. Lima, V. LeRhun, F. Delime, C. Coutanceau, F.M. Léger, *J. Power Sources* 105 (2002) 283.
- [14] Z. Chen, L. Xu, W. Li, M. Waje, Y. Yan, *Nanotechnology* 17 (2006) 5254.
- [15] S. Guo, S. Dong, E. Wang, *Small* 5 (2009) 1869.
- [16] B. Rajesh, K.R. Thampi, J.M. Bonard, H.J. Mathieu, N. Xanthopoulos, B. Viswanathan, *Electrochem. Solid State Lett.* 7 (2004) A404.
- [17] B. Rajesh, K.R. Thampi, J.M. Bonard, H.J. Mathieu, N. Xanthopoulos, B. Viswanathan, *Chem. Commun.* (2003) 2022.
- [18] X. Feng, C. Mao, G. Yang, W. Hou, J. Zhu, *Langmuir* 22 (2006) 4384.
- [19] P. Xu, X. Han, B. Zhang, N.H. Mack, S. Jeon, H.L. Wang, *Polymer* 50 (2009) 2624.
- [20] H.H. Zhou, S.Q. Jiao, J.H. Chen, W.Z. Wei, Y.F. Kuang, *J. Appl. Electrochem.* 34 (2004) 455.
- [21] F. Liu, L. Huang, T. Wen, C. Li, S. Huang, *Synth. Met.* 158 (2008) 767.
- [22] E. Antolini, E.R. Gonzalez, *Appl. Catal. A: Gen.* 365 (2009) 1.
- [23] J.H. Choi, Y.M. Kim, J.S. Lee, K.Y. Cho, H.Y. Jung, J.K. Park, I.S. Park, Y.-E. Sung, *Solid State Ionics* 176 (2005) 3031.
- [24] C.W. Lin, R. Thangamuthu, C.J. Yang, *J. Membr. Sci.* 253 (2005) 23.
- [25] Y.F. Huang, C.W. Lin, *Polymer* 50 (2009) 775.
- [26] Y.F. Huang, C.W. Lin, *Synth. Met.* 159 (2009) 1824.
- [27] Y.F. Huang, C.W. Lin, *Synth. Met.* 160 (2010) 384.
- [28] Y.F. Huang, C.W. Lin, *Polym. Int.* 59 (2010) 1226.
- [29] T.C. Wen, L.M. Huang, A. Gopalan, *J. Electrochem. Soc.* 148 (2001) D9.
- [30] W.C. Chen, T.C. Wen, A. Gopalan, *J. Electrochem. Soc.* 148 (2001) E427.
- [31] L. Liang, J. Liu, C.F. Windisch, G.J. Exarhos, Y.H. Lin, *Angew. Chem. Int. Ed.* 41 (2002) 3665.
- [32] J. Stejskal, I. Sapurina, M. Trchová, E.N. Konyushenko, *Macromolecules* 41 (2008) 3530.
- [33] J. Huang, R.B. Kaner, *J. Am. Chem. Soc.* 126 (2004) 851.
- [34] X.C. Wang, S.J. Ding, J. Cao, F.L. Wu, C. Zhou, Z.Z. Yang, *Chin. Chem. Lett.* 16 (2005) 1523.
- [35] H. Lee, S.E. Habas, S.K.D. Butcher, G.A. Somorjai, P. Yang, *Angew. Chem.* 118 (2006) 7988.
- [36] J. Zhao, W. Chen, Y. Zheng, *Mater. Chem. Phys.* 113 (2009) 591.
- [37] Q. Jiang, X. Wu, M. Shen, Z. Ma, X. Zhu, *Catal. Lett.* 124 (2008) 434.
- [38] W. Chen, J. Zhao, J.Y. Lee, Z. Liu, *Mater. Chem. Phys.* 91 (2005) 124.
- [39] J. Chen, Y. Jin, *Adv. Mater. Res.* 96 (2010) 55.
- [40] N. Toshima, T. Yonezawa, *New J. Chem.* 22 (1998) 1179.
- [41] X. Yan, H. Liu, K.Y. Liew, *J. Mater. Chem.* 11 (2001) 3387.
- [42] T. Yajima, H. Uchida, M. Watanabe, *J. Phys. Chem. B* 108 (2004) 2654.
- [43] Y.M. Zhu, H. Uchida, T. Yajima, M. Watanabe, *Langmuir* 17 (2001) 146.
- [44] A. Lenoe, W. Marino, B.R. Scharifker, *J. Electrochem. Soc.* 139 (1992) 438.
- [45] Q.L. Zhong, W.H. Li, Z.Q. Tian, *Acta Phys. Chim. Sin.* 10 (1994) 813.